Renormalization of the Graphene Dispersion Velocity Determined from Scanning Tunneling Spectroscopy

Jungseok Chae, Suyong Jung, Andrea F. Young, Cory R. Dean, Lei Wang, Yuanda Gao, Kenji Watanabe, Takashi Taniguchi, James Hone, Kenneth L. Shepard, Phillip Kim, Nikolai B. Zhitenev, and Joseph A. Stroscio

Phys. Rev. Lett. **109**, 116802 — Published 11 September 2012

DOI: 10.1103/PhysRevLett.109.116802

Renormalization of the Graphene Dispersion Velocity Determined from Scanning Tunneling Spectroscopy

Jungseok Chae[1,2], Suyong Jung[1,2,3], Andrea F. Young[4], Cory R. Dean[5,6], Lei Wang[6], Yuanda Gao[6], Kenji Watanabe[7], Takashi Taniguchi[7], James Hone[6], Kenneth L. Shepard[5], Philip Kim [4], Nikolai B. Zhitenev[1*], and Joseph A. Stroscio[1*]

[1]Center for Nanoscale Science and Technology, National Institute of Standards and Technology, Gaithersburg, MD 20899, USA
[2]Maryland NanoCenter, University of Maryland, College Park, MD 20472, USA
[3]Korea Research Institute of Standards and Science, Daejeon, 305-340 Korea
[4]Department of Physics, Columbia University, New York, NY 10027, USA
[5]Department of Electrical Engineering, Columbia University, New York, NY 10027, USA
[6]Department of Mechanical Engineering, Columbia University, New York, NY 10027, USA
[7]Advanced Materials Laboratory, National Institute for Materials Science, Tsukuba, Ibaraki 305-0047 Japan

In graphene, as in most metals, electron-electron interactions renormalize the properties of electrons but leave them behaving like non-interacting quasiparticles. Many measurements probe the renormalized properties of electrons right at the Fermi energy. Uniquely for graphene, the accessibility of the electrons at the surface offers the opportunity to use scanned probe techniques to examine the effect of interactions at energies away from the Fermi energy, over a broad range of densities, and on a local scale. Using scanning tunneling spectroscopy, we show that electron interactions leave the graphene energy dispersion linear as a function of excitation energy for energies within ±200 meV of the Fermi energy. However, the measured dispersion velocity depends on density and increases strongly as the density approaches zero near the charge neutrality point, revealing a squeezing of the Dirac cone due to interactions.

In the absence of interactions the low energy excitations in graphene are described by massless Dirac quasiparticles with a linear energy-momentum dispersion, $E = \hbar v k$, where the constant of proportionality is the carrier group velocity, v. When many-body interactions are included, the energy dispersion can change [1–12]. In general, this change depends on the parameters $[n, k, r_s]$, where n is the carrier density, k is the momentum relative to the Brillouin zone corner, and r_s is the interaction parameter or coupling constant describing the relative strength of the Coulomb interactions and is given by the ratio of potential to kinetic energies [13]. In graphene, both the kinetic and potential energies scale as the square root of the density, so that r_s is independent of density. Therefore, in graphene, the dependence of the dispersion renormalization on r_s and n can be separated. For monolayer graphene r_s is given by $r_s = e^2 / 4\pi\varepsilon_0\varepsilon_m\hbar v$, where e is the electron charge, $\hbar$ is Planck's constant divided by 2π, ε_0 is the permittivity of free space, and ε_m is the effective dielectric constant of the medium in which the graphene sheet is embedded.

Previously, measurements of the graphene dispersion renormalization have either examined solely the density dependence [11] or the dependence on energy [6,9,10], but not both over wide ranges of density and energy due to limitations in experimental techniques. Transport measurements, which are sensitive to the behavior of electrons at the Fermi energy (E_F), have shown the dispersion velocity at E_F increases at low density [11]. Angle-resolved photoemission spectroscopy (ARPES) has examined the energy dependence of the dispersion and found deviations from linearity at high energies below approximately -0.4 eV [9]. ARPES measurements are complicated by the appearance of plasmonic and phonon structures which can distort the spectrum at the Dirac point [6], and they have not been able to examine the density

dependence in detail due to the lack of large area gated graphene devices. Scanning tunneling spectroscopy measurements of back-gated devices allows the graphene dispersion to be examined as a function of energy away from the Fermi energy [8,14] so that the renormalization can be determined separately as a function of excitation energy and density.

For excitations at the Fermi level *i.e.* at $k = k_F$, many-body theory predicts that the renormalized spectrum of graphene can be characterized by a velocity v^* given by [1–3],

$$\frac{v^*}{v} = 1 - \frac{r_s}{\pi}\left[\frac{5}{3} + \ln(r_s)\right] + \frac{r_s}{8}\ln\left(\frac{n_C}{n}\right) \quad (1)$$

The Fermi velocity enhancement described in Eq. (1) was calculated within the random phase approximation (RPA), where v is the bare dispersion velocity in the absence of interactions and n_C is a density corresponding to the ultraviolet cutoff energy, which is ≈ 3 eV [2,11]. The 2nd and 3rd terms in Eq. 1 result from intraband and interband contributions, respectively. The expression in Eq. 1 describes the reshaping of the Dirac cone at energies equal to the Fermi energy E_F. Velocity enhancements obtained from Shubnikov de Haas oscillations in transport measurements have considered only the interband contribution in Eq. (1), and found the need for an additional density dependent parameter to get agreement with experiment [11]. The question on how the dispersion velocity depends on energy over a broad range of densities remains open.

In this Letter, we present the first experimental measurements of the Landau level (LL) spectroscopy of graphene on hexagonal boron nitride (hBN) spacer layers. The lower disorder in graphene with hBN spacer layers allows a significant improvement in LL lifetimes, with the appearance of many LLs over a wide energy range. This enhanced spectrum, compared to previous results without hBN [8,14], allows us to separate the energy and density contributions

to the renormalization of the graphene band structure. We show how to quantitatively examine the Landau level tunneling spectrum taking into account probe tip and graphene quantum capacitances and to extract interaction driven velocity renormalization with good accuracy. We find that interactions do not significantly distort the Dirac cones at low energies. Instead, they preserve the linear dispersion while parametrically renormalizing the dispersion velocity at a given fixed density. The measured renormalized velocity is satisfactorily described by the RPA theory incorporating the interaction strength r_s and the ultra-violet cutoff density n_c [2,12] described by Eq. (1) without the need of additional parameters.

The experiments were performed in a custom designed cryogenic scanning tunneling microscope system operating at 4 K with applied magnetic fields from 0 T to 8 T [15]. The graphene devices were fabricated by the method detailed in Dean *et al*. [16]. A heavily doped silicon substrate was used as a back gate to control the carrier density n in the sample by applying back gate voltage V_G. In our experiments, a bias voltage V_B is applied to the graphene and the tunneling current I is measured from the tip to obtain tunneling spectra dI/dV as a function of V_B, V_G, and applied magnetic field B. Topography measurements of graphene on hBN (Fig. 1(a)) are characterized by a moiré pattern formed by the relative rotation of the graphene sheet with respect to the underlying hBN crystal as observed in previous studies [17,18]. The topographic modulation in Fig. 1(a) is consistent with the thin BN spacer layer (5 nm) used in these studies [16].

Upon applying a magnetic field, the tunneling spectra develops sharp peaks as a function of V_B as shown in Fig 1(b), indicating the formation of the Landau levels (LL) [14,19–21]. The reduced disorder in graphene on hBN is evident by the high fidelity of the LL formation compared to previous measurements on SiO_2 [8,14]. The LL index N can be identified from the

peak distance in bias V_B compared to the expected LL energy spectra proportional to $|N|^{1/2}$. The widths of the LLs, determined by the lifetime of the Dirac quasiparticles, approaches those measured in the low-disorder graphene grown epitaxially on SiC [19,21]. Figure 1(c) shows the map of the N = -1 LL peak position, which reflects the spatial variation of disorder potential. Within the area of interest, two local potential extrema are indicated as A and B. At low density, A becomes an electron puddle (blue) while B a hole puddle (yellow).

The tunneling spectra in Fig. 1(b) reflect the graphene LL density of states at a gate voltage of V_G = -30 V, which induces additional holes to lower the Fermi level by ≈ 200 meV with respect to the Dirac point. Repeating the same tunneling spectra measurements while varying the back gate voltage, thus controlling the relative positions of the Fermi level and the Dirac point, we can obtain a complete data set, which we refer to as a "gate map". The resulting tunneling spectra, represented in a two dimensional plot of V_B and V_G, are shown in Fig. 2, (a) and (b), for 2 T and 5 T, respectively. The LL spectra variation as a function of energy and density can be investigated by tracing peaks of the tunneling spectra (bright curve traces) in these gate maps. At lower magnetic field, Fig. 2(a), the smooth curvature of the LLs with gate voltage approximately corresponds to the energy variation of the charge neutrality point (Dirac point), which varies as $E_D \propto n^{1/2}$. In larger fields (Fig. 2(b)) LL formation leads to the familiar stair case pattern in the gate maps, previously seen in graphene on SiO_2 [8,14], or GaAs 2DEGs [22]. Every LL becomes pinned at the Fermi level until it fills with carriers and upon filling the next unfilled LL makes a quick transition to become pinned at E_F.

To accurately analyze the energy dispersion, we simulate the single particle properties in the gate maps (Fig. 2(c)) by calculating the tunneling conductance spectral map using a capacitor model [23] that includes the graphene-back-gate capacitance (C_G), graphene-probe capacitance

(C_P), the graphene quantum capacitance, and a constant velocity v. The simulation in Fig. 2(c) shows that the LL staircase transitions do not occur at fixed V_G but at different values as V_B changes, appearing as a line with an angle in the gate map. This angle is due to the local gating of the graphene by the bias potential between the probe tip and graphene, and is determined by the ratio of the back gate and probe capacitances, C_G/C_P. The constant density (or constant chemical potential) axis is therefore along the LL transitions given by this capacitance ratio, as indicated by the red line in Fig. 2(b). For a better comparison, we simulate the LL spectra in the V_G and V_B maps by considering a fixed v and a smoothly varying C_G/C_P ratio determined from the experimental gate maps [24], as shown in Fig. 2(c). The simulation result matches well the experimental LL transitions and indicates the simulation captures the single particle physics. Departure from single particle behavior due to many body effects is seen by a comparing the simulation with the experiment at low densities. Deviations from the constant-velocity simulation are illustrated by overlapping the simulation from Fig. 2(c) onto Fig. 2(b) (yellow overlay) in the regions of high density and near the charge neutrality point. Very good agreement is seen in matching the LL energy peak positions at high density. However, the simulated LL peak positions underestimate the experimental positions and significantly deviate at low density indicating that the dispersion velocity is larger close to the charge neutrality point. For example, the simulated peak position of LL_2 lies in the minimum of the spectrum between the peaks of LL_1 and LL_2 at zero gate voltage (see white arrow in Fig. 2(b)).

To accurately determine the interaction driven velocity enhancements, we define a constant density (or chemical potential) axis in the (V_B, V_G) space using the transitions of the LLs, which is determined from the C_G/C_P ratio [24]. Therefore the LL energy E_N can be obtained at a fixed density for the Nth LL (LL_N) by measuring the LL spectral peak positions in

the plateau regions along lines of constant density (red line in Fig. 2(b)) thereby converting $dI/dV(V_B, V_G)$ to $dI/dV(E,n)$. A comparison of the dI/dV spectra at constant V_G vs. constant density n (Fig. 3(a)) shows that the spectrum at constant gate voltage overestimates the energy scale by as much as 5 % leading to a corresponding error in an estimate of the dispersion velocity. The importance of examining the correct LL_N peak energies at constant density is compounded by the fact that the energy scale error at constant gate voltage varies with density, since the C_G/C_P ratio varies. This will result in errors as large 30 % in determining r_s parameters from the velocity incorrectly determined at constant gate voltage. Below we determine the many body corrections to the renormalized velocity by correctly analyzing the LL spectra at constant density with a correct energy scale [24].

In graphene, the linear dispersion yields the LL spectra, $E_N = E_D + \mathrm{sgn}(N)\hbar v\sqrt{NB}$. The LL spectroscopy presented in Fig. 2 thus allows us to probe the dispersion velocity at fixed density and magnetic field by inspecting E_N for different N (Fig. 3(a)). Figure 3(b) shows E_N-E_D vs. $\sqrt{NB}$ for different density values. Here E_D is obtained from $E_{N=0}$ at a given density. A remarkable feature in Fig. 3(b) is that the LL dispersion is highly linear (see inset in Fig. 3(b)) at a fixed density but changes slope as the density decreases. The energy dispersion is thus described by the Dirac cone in this energy range but the cone is *squeezed* at low density, as schematically illustrated in Fig. 4(a).

The velocity extracted from the LL dispersion fits is shown in Fig. 4(b) as a function of density for the electron and hole puddle locations, A and B. We observe a significant increase in velocity near the charge neutrality point. We fit the renormalized velocity using Eq. (1). The solid line in Fig. 4(b) shows a two parameter fit, to the combined data of puddles A and B, with a

bare velocity $v = (0.957 \pm 0.003) \times 10^6$ m/s and an interaction parameter $r_s = 0.69 \pm 0.03$ [25]. The bare velocity is in agreement with previous measurements by a large number of different experiments [19,21,26–29]. The fit parameter r_s is equivalent to a measurement of the effective dielectric constant of $\varepsilon_{BN/SiO_2} = 5.3 \pm 0.3$ [25], using $\varepsilon_m = (\varepsilon_{BN/SiO_2} + 1)/2$.

In summary, we present measurements of the LL density of states of graphene on hBN as a function of spatial position, density, and magnetic field. Tunneling spectroscopy at energies away from E_F allow us to separately analyze the graphene dispersion dependence on excitation energy and density. The dispersion of the LLs as a function of orbital index shows that the linear graphene energy-momentum dispersion is retained at low energies even as the charge neutrality point is approached. However, electron interactions cause an increase of the dispersion velocity, effectively squeezing the Dirac cone, with decreasing density in agreement with recent theoretical predictions [12].

We thank S. Das Sarma, S. Adam, and M. D. Stiles for valuable discussions, and S. Blankenship and A. Band for technical assistance. J.C. and S.J. acknowledges support under the Cooperative Research Agreement between the University of Maryland and the National Institute of Standards and Technology Center for Nanoscale Science and Technology, Award 70NANB10H193, through the University of Maryland. Columbia work is supported by AFOSR MURI, and FCRP through C2S2 and FENA, P.K and A. Y. F. thank NRI INDEX program for their support.

*To whom correspondence should be addressed: nikolai.zhitenev@nist.gov, joseph.stroscio@nist.gov .

Figure Captions:

Figure 1. Local probing of graphene on hBN. (a) STM topographic image of graphene on hBN. The moiré pattern with a unit cell length of 4.5 nm, corresponds to a rotation of 3.1˚ of the graphene lattice relative to the hBN cystal. (b) Differential conductance spectra of graphene on hBN at $V_G = -30$ V. (c) Spatial variation of the $N = -1$ LL peak position measured in the same area as (a), reflecting the local disorder potential variation. The positions A and B (white dots) denote electron and hole puddle locations where measurements are reported in Figs. 2-4.

Figure 2. Gate mapping tunneling spectroscopy of the Landau level density of states of graphene on hBN. Each map is built of individual *dI/dV* vs. V_B spectra taken at multiple fixed V_G. The color scale is the *dI/dV* magnitude. (a) *dI/dV* gate map at $B = 2$ T obtained in the hole puddle labeled B in Fig. 2(c). (b) *dI/dV* gate map spectra at $B = 5$ T. The red line indicates an axis of constant density (chemical potential) following the transitions of the LLs as discussed in the text, while the blue line indicates constant V_G. The yellow overlays are portions of the simulation in (c). (c) Simulation of the *dI/dV* gate map spectra at $B = 5$ T with a constant dispersion velocity of 1.1×10^6 m/s and the probe-sample capacitance determined from the slope of the LL transitions in (b) [24]. Portions of the simulation are overlaid in (b) (yellow lines) showing agreement at high densities and deviations at low densities from using a constant velocity. The white arrow points to the simulated LL_2 position which lies in between the experimental LL_1 and LL_2 peaks at low density.

Figure 3. Landau level dispersion. (a) *dI/dV* spectra (red) at constant density obtained along the red line in Fig. 2(b). A fit of LL peaks $N = 1$ to $N = 6$ is shown in green using a series of Lorentzians. (inset) A comparison of the *dI/dV* spectra at constant gate voltage ($V_G = 12$ V) (blue) and constant density (red), obtained along the lines indicated in Fig. 2(b). The spectra at constant gate voltage overestimates the energy scale by 5 % at this density. (b) Determination of the graphene dispersion velocity from the LL peak energy positions (obtained along lines of constant density in the gate maps) for the electron puddle A at $B = 2$ T. The peak positions are plotted as a function of square root of the Landau orbital index N and magnetic field B. A linear fit (solid lines) is used to determine the dispersion velocity. (inset) Residuals from the linear fit showing very good linearity in the LL dispersion.

Figure 4. Renormalized graphene dispersion. (a) Schematic of the Dirac cone variation as a function of density. The data presented in this paper shows that the graphene energy-momentum dispersion remains linear at low energy in the presence of electron interactions, while the Dirac cone angle, which is inversely proportional to the velocity, decreases (gets squeezed) at low density. (b) Renormalized velocity determined from the linear fitting of LL peak positions as described in Fig. 3(b) as a function of density for the electron (red symbols) and hole (blue symbols) puddle locations A and B at $B = 2$ T. The solid line shows a fit to the combined data from puddle A and B using Eq. (1) with $v = (0.957 \pm 0.003) \times 10^6$ m/s and $r_s = (0.69 \pm 0.03)$ [25].

References:

[1] J. González, F. Guinea, and M. A. H. Vozmediano, Phys. Rev. B **59**, R2474 (1999).
[2] S. Das Sarma, E. H. Hwang, and W.-K. Tse, Phys. Rev. B **75**, 121406 (2007).
[3] M. Polini, R. Asgari, Y. Barlas, T. Pereg-Barnea, and A. H. MacDonald, Solid State Commun. **143**, 58–62 (2007).
[4] D. E. Sheehy and J. Schmalian, Phys. Rev. Lett. **99**, 226803 (2007).
[5] E. H. Hwang and S. Das Sarma, Phys. Rev. B **77**, 081412 (2008).
[6] A. Bostwick *et al.*, Science **328**, 999 (2010).
[7] F. de Juan, A. G. Grushin, and M. A. H. Vozmediano, Phys. Rev. B **82**, 125409 (2010).
[8] A. Luican, G. Li, and E. Y. Andrei, Phys. Rev. B **83**, 041405 (2011).
[9] D. A. Siegel *et al.*, PNAS **108**, 11365 (2011).
[10] A. L. Walter *et al.*, Phys. Rev. B **84**, 085410 (2011).
[11] D. C. Elias *et al.*, Nat. Phys. **7**, 701 (2011).
[12] S. D. Sarma and E. H. Hwang, arXiv:1203.2627 (2012).
[13] S. Das Sarma, S. Adam, E. H. Hwang, and E. Rossi, Rev. Mod. Phys. **83**, 407 (2011).
[14] S. Jung *et al.*, Nat. Phys. **7**, 245 (2011).
[15] J. A. Stroscio, E. W. Hudson, S. R. Blankenship, R. J. Celotta, and A. P. Fein, Proceedings of SPIE **4608**, 112–115 (2002).
[16] C. Dean *et al.*, Nat. Nano. **5**, 722 (2010).
[17] J. Xue *et al.*, Nat. Mater. **10**, 282 (2011).
[18] R. Decker *et al.*, Nano Letters **11**, 2291 (2011).
[19] D. L. Miller *et al.*, Science **324**, 924 (2009).
[20] G. Li, A. Luican, and E. Andrei, Phys. Rev. Lett. **102**, 176804 (2009).
[21] Y. J. Song *et al.*, Nature **467**, 185 (2010).
[22] O. E. Dial, R. C. Ashoori, L. N. Pfeiffer, and K. W. West, Nature **448**, 176 (2007).
[23] C. E. Malec and D. Davidović, J. Appl. Phy. **109**, 064507 (2011).
[24] The tip-graphene capacitance has the following effects. First, the graphene density is affected by finite tunneling bias. As a result, the lines of constant density are tilted in the gate maps. The slope of the lines depends on gate voltage due to the variation in the screening properties of graphene with density, which affects the capacitance C_P. From the measured slope of the LL transitions in the gate map, we determine the slopes of constant density are well described by for all fields below 5 T by $C_G/C_P = A + B(V_G - C)^2$, where $A = 0.068$, $B = 7.36 \times 10^{-5}$, and $C = -7.91$. Second, the density scale has to be corrected even at zero tip bias because of the quantum capacitance of graphene. The density axis is properly corrected based the complete simulation mainly resulting in approximately a 5 % reduction in density at the highest gate voltages.
[25] The uncertainties in the renormalized velocities in Fig. 4(b) are a single standard deviation as determined from a linear fit to the LL level peak dispersions, as shown in Fig. 3(b). The reported uncertainty in v and r_s is a single standard deviation as determined from the non-linear least squares fitting of the data in Fig. 4(b). The reported error in ε_{BN} is the error in r_s propagated in calculating ε_{BN}.
[26] K. S. Novoselov *et al.*, Nat. Phys. **2**, 177 (2006).
[27] Y. Zhang, Y.-W. Tan, H. L. Stormer, and P. Kim, Nature **438**, 201 (2005).
[28] M. Orlita *et al.*, Phys. Rev. Lett. **101**, 267601 (2008).

[29] J. Martin *et al.*, Nat. Phys. **5**, 669 (2009).

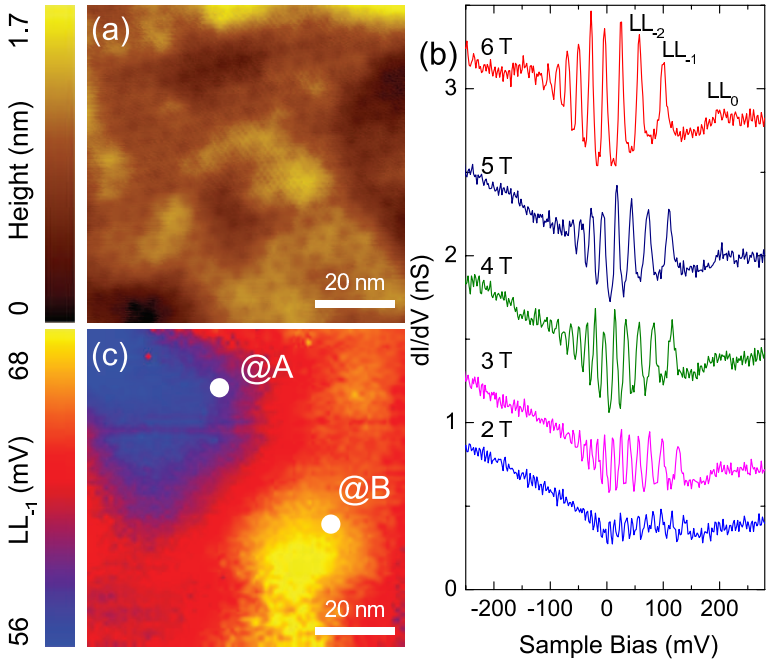

Fig. 1. Local probing of graphene on h-BN. (a) STM topographic image of graphene on hBN. The moiré pattern with a unit cell length of 4.5 nm, corresponds to a rotation of 3.1˚of the graphene lattice relative to the hBN crystal. (b) Differential conductance spectra of graphene on hBN at V_G=–30 V. (c) Spatial variation of the N=1 LL peak position measured in the same area as (a), reflecting the local disorder potential variation. The positions A and B (white dots) denote electron and hole puddle locations where measurements are reported in Figs. 2-4.

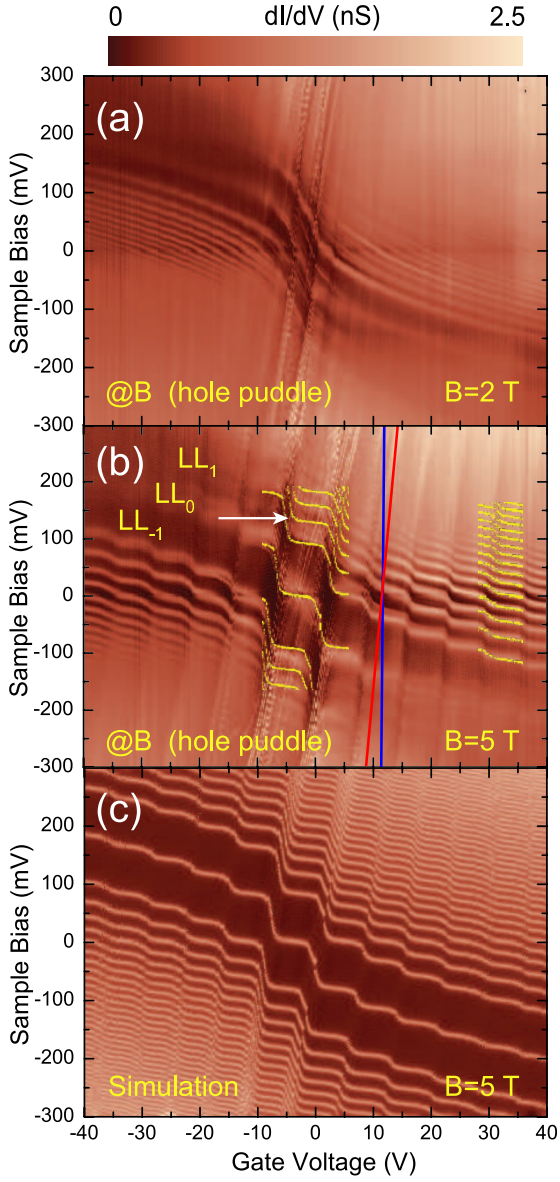

Fig. 2. Gate mapping tunneling spectroscopy of the Landau level density of states of graphene on h-BN. Each map is built of individual *dI/dV* vs. V_B spectra taken at multiple fixed V_G. The color scale is the *dI/dV* magnitude. (a) *dI/dV* gate map spectra showing the Landau levels at $B = 2$ T obtained in the hole puddle labeled B in Fig. 2(c). (b) *dI/dV* gate map spectra at $B = 5$ T. The red line indicates an axis of constant density (chemical potential) following the transitions of the LLs as discussed in the text, while the blue line indicates constant V_G. The yellow overlays are portions of the simulation in (c). (c) Simulation of the d*I*/d*V* gate map spectra at $B = 5$ T with a constant dispersion velocity of 1.1×10^6 ms^{-1} and the probe-sample capacitance determined from slope of the LL transitions in (b) [24]. Portions of the simulation are overlaid in (b) (yellow lines) showing agreement at high densities and deviations at low densities from using a constant velocity. The white arrow points to the simulated LL_2 position which lies in between the experimental LL_1 and LL_2 peaks at low density.

Figure 2 LU13549 10AUG2012

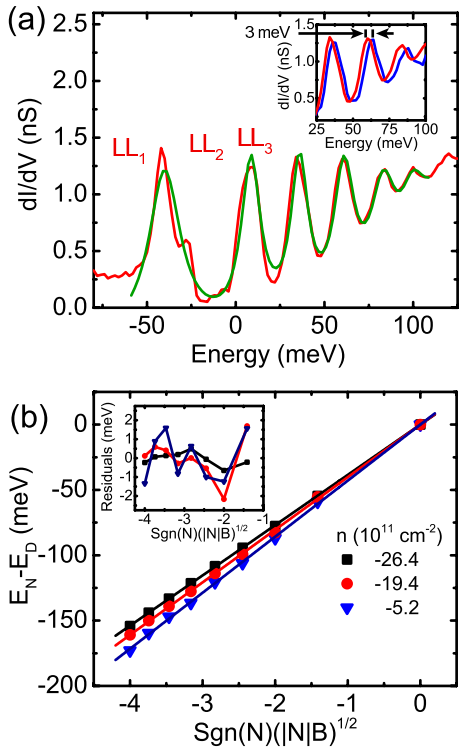

Fig. 3. Landau level dispersion. (a) dI/dV spectra (red) at constant density obtained along the red line in Fig. 2(b). A fit of LL peaks N=1 to N=6 is shown in green using a series of Lorentzians. (inset) A comparison of the dI/dV spectra at constant gate voltage (V_G=12 V) (blue) and constant density (red), obtained along the lines indicated in Fig. 2(b). The spectra at constant gate voltage overestimates the energy scale by 5% at this density. (b) Determination of the graphene dispersion velocity from the LL peak energy positions (obtained along lines of constant density in the gate maps) for the electron puddle A at B=2 T. The peak positions are plotted as a function of square root of the Landau orbital index N and magnetic field B. A linear fit (solid lines) is used to determine the dispersion velocity. (inset) Residuals from the linear fit showing very good linearity in the LL dispersion.

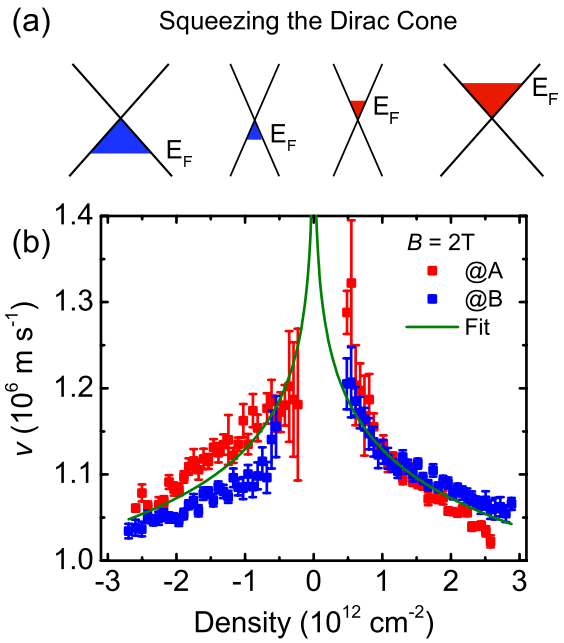

Fig. 4. Renormailzed graphene dispersion. (a) Schematic of the Dirac cone variation as a function of density. The data presented in this paper shows that the graphene energy-momentum remains linear at low energy in the presence of electron interactions, while the Dirac cone angle, which is inversely proportional to velocity, decreases (gets squeezed) at low density. (b) Renormalized velocity determined from the linear fitting of LL peak positions as described in Fig. 3(b) as a function of density for the electron (red symbols) and hole (blue symbols) puddle locations A and B at B= 2 T. The solid line shows a fit to the combined data set using Eq. 1 with v=(0.957±0.003) x10^6 ms^{-1} and r_S=(0.69±0.03) [25].